$Ca_6Li_xAl_{23-x}$, $Sr_9Li_{7+x}Al_{36-x}$, and $Ba_2Li_{3+x}Al_{6-x}$: New Ternary Intermetallic Compounds Linking Close-Packed Metal Structures and Zintl Phases

Ulrich Häussermann,*,† Michael Wörle, and Reinhard Nesper

Contribution from the Laboratory of Inorganic Chemistry, ETH-Zürich, Universitätstr. 6, CH-8092 Zürich, Switzerland

Received April 5, 1996[⊗]

Abstract: Investigations of the ternary systems M/Li/Al of the heavier alkaline earth metals M = Ca, Sr, Ba yielded three new intermetallic compounds which show interesting structural relationships. $Ca_6Li_xAl_{23-x}$ ($x \approx 11$, $Fm\bar{3}m$, $a = 13.430(2)$ Å, $Z = 4$) crystallizes in the Th_6Mn_{23} structure with all sites of the majority component occupied by Li and Al. $Sr_9Li_{7+x}Al_{36-x}$ ($x \approx 10.5$, $P6_3/mmc$, $a = 9.638(4)$ Å, $c = 27.586(6)$ Å, $Z = 2$) is a relative of the Sr_3Mg_{13} structure, and $Ba_2Li_{3+x}Al_{6-x}$ ($x \approx 1.2$, $R\bar{3}m$, $a = 9.946(1)$ Å, $c = 26.992(3)$ Å, $Z = 9$) is a hexagonal relative of the Th_6Mn_{23} type. The substructures formed by Li and Al atoms are described in terms of two simple basis clusters which offer structural flexibility in their connectivity. The relative stability of the substructures has been investigated within the simple tight-binding Hückel model. Calculated energy difference curves as a function of the valence electron concentration for these networks show a pronounced stability maximum in the region of 2.5−2.7 electrons per network atom. This result fits the composition of the intermetallic compounds when applying the Zintl−Klemm concept. In addition, Mulliken population analyses of extended Hückel calculations have been used to investigate the site occupancies.

1. Introduction

A distinctive characteristic of main group intermetallics is their structural diversity, and very often it appears to be difficult to find the structural principles and thus a deeper understanding of the structural chemistry of this exciting class of chemical compounds.[1] Binary intermetallic compounds A_mB_n formed between Mg or Li (B component) and one of the heavier alkaline earth metals, Ca, Sr, or Ba, are one example. When the *n*/*m* ratio is between 3.8 and 5.2, they form a remarkable family of related structures. Four different structure types are known to occur within this range of composition: the hexagonal structures of $BaLi_4$,[2] Sr_3Mg_{13},[3] and $SrMg_{5.2}$[4] ($EuMg_{5.2}$ type) as well as the cubic Th_6Mn_{23} structure type[5] with the representatives Sr_6Li_{23}, Sr_6Mg_{23}, and Ba_6Mg_{23}.[6] Characteristically, the B component forms a network structure with large voids in which noncentered A_6 octahedra and/or A_3 triangles are located. As a starting point for an interpretation of these structures, it is attractive to divide them into an electropositive A part and a B substructure similar to Zintl phases and further probe a possible relationship between the valence electron concentration (VEC) and the geometrical structure of the B substructures.

In this article we report two novel structures of the compounds $Ba_2Li_{3+x}Al_{6-x}$ ($x \approx 1.21$) and $Sr_9Li_{7+x}Al_{36-x}$ ($x \approx 10.5$), which are closely related to the Th_6Mn_{23} and the Sr_3Mg_{13} structure type, respectively. These structures exhibit a B network which is formed by Li and Al atoms together, and sites may have mixed Li/Al occupation as well as purely be occupied by one sort of atom. Additionally, we present the compound $Ca_6Li_xAl_{23-x}$ ($x \approx 11$) which crystallizes as a variant of the Th_6Mn_{23} structure type. Interestingly we found that the B substructures of the known binary and the new ternary compounds can be described in terms of two simple basis clusters and structural variety results from the possibility of connecting these clusters in different ways. Furthermore we observed that the VEC has a strong influence on the structural stability of the sp-bonded B substructures in this class of intermetallic compounds. The calculated optimum VEC is around 2.5 electrons per B atom, and this closes a gap between the VEC typically occurring in sp-bonded close-packed structures (VEC ≤ 2) and polyanionic substructures of polar intermetallic compounds and Zintl phases (VEC > 3.5) (Figure 1). We defined the VEC as the number of valence electrons per electronegative B atom in the spirit of the Zintl−Klemm concept. Thus the VEC of a compound A_mB_n is calculated by dividing the number of valence electrons per formula unit by the number of B atoms.

2. Structural Relationships

A structural relationship between the Th_6Mn_{23}, Sr_3Mg_{13}, and $EuMg_{5.2}$ structure types was pointed out by Erassme and Lueken on the basis of stacking units of the A clusters with a suitable B coordination shell.[3] From recent quantum mechanical investigations of selected intermetallic phases, we know that the leading interactions are between B type atoms and that the heavier earth alkaline elements tend to transfer a considerable amount of charge density to the B framework.[7,8] We thus use an alternative description which starts with a partitioning of the B substructures into basis clusters, namely tetrahedral and double

† Present address: Inorganic Chemistry 2, University of Lund, P.O. Box 124, S-22100 Lund, Sweden.

⊗ Abstract published in *Advance ACS Abstracts,* November 1, 1996.

(1) Nesper, R. *Angew. Chem., Int. Ed. Engl.* **1991**, *30*, 789.
(2) Kanda, F. A.; Miskell, C. F.; King, A. J. *Acta Crystallogr.* **1965**, *18*, 24.
(3) Erassme, J.; Lueken, H. *Acta Crystallogr.* **1987**, *B43*, 225.
(4) Erassme, J.; Brauers, T.; Lueken, H. *J. Less-Common Met.* **1988**, *137*, 155.
(5) Florio, J.; Rundle, R. E.; Snow, I. A. *Acta Crystallogr.* **1952**, *5*, 449.
(6) Villars, P.; Calvert, L. D. *Pearsons Handbook of Crystallographic Data for Intermetallic Compounds*, 2nd ed.; ASM International: Materials Park, OH, 1991.
(7) Häussermann, U.; Wengert, S.; Hofmann, P.; Savin, A.; Jepsen, O.; Nesper, R. *Angew. Chem., Int. Ed. Engl.* **1994**, *33*, 2069.
(8) Häussermann, U.; Wengert, S.; Nesper, R. *Angew. Chem., Int. Ed. Engl.* **1994**, *33*, 2073.

S0002-7863(96)01127-4 CCC: $12.00

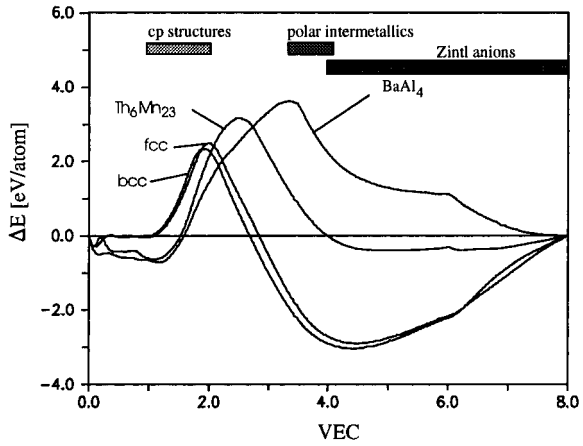

Figure 1. Energy difference curves between the B substructures in $BaAl_4$ and Th_6Mn_{23}, the close-packed structures fcc and bcc, and the simple cubic structure as a reference obtained by means of TB calculations with second-moment scaling.[15] For positive values of ΔE, a structure is more stable than the reference structure (baseline with $\Delta E = 0$). The chosen reference value of the second moment was the mean value for the Al substructure in $BaAl_4$ and for fcc-Al in their equilibrium volumes. The ranges of preferred values of VEC (number of valence electrons per (electronegative) atom) in close-packed (cp) sp-bonded structures and in polyanions of polar intermetallics and Zintl phases are emphasized.

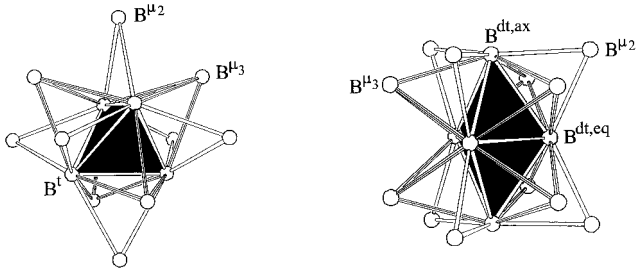

Figure 2. Tetrahedral star with coordination of the edges of the central tetrahedron (black) by B^{μ_2} atoms (left) and double tetrahedral star with the $B^{dt,eq}-B^{dt,ax}$ edges of the central trigonal bipyramid (black) bridged by B^{μ_2} atoms (right).

tetrahedral stars. A tetrahedral star (TS) (after Tetraederstern[9]) consists of a central tetrahedron (built of the B^t atoms) with all faces coordinated in a μ_3 fashion (by the B^{μ_3} atoms) leading to an arrangement of four tetrahedra linked facially to the central tetrahedron. The double tetrahedral star (DTS) has a trigonal bipyramid as the central polyhedron (with the B^{dt} atoms as vertices) and all faces capped. In the observed B substructures, these basis clusters are linked via a third type of B atom bridging all edges of the central tetrahedron in a tetrahedral star and the edges formed between equatorial and axial B^{dt} atoms in a double tetrahedral star. Each of those μ_2 coordinated atoms (B^{μ_2}) connect two basis clusters. The final cluster units have the formulas ($B^t_4B^{\mu_3}_4B^{\mu_2}_{6/2}$) and ($B^{dt}_5B^{\mu_3}_6B^{\mu_2}_{6/2}$) and are shown in Figure 2.

The projection on a plane perpendicular to the 3-fold axis of these units is the same for both (Figure 3). In all three structure types the basis clusters are arranged in hexagonal close-packed layers (Figure 4) with an orientation exhibited in the projection drawn in Figure 3. Triangles of the bigger A atoms are situated within a hexagonal layer. Layers consisting of DTS contain additional B atoms. This sort of B atom ($B^{st,DTS}$) stuffs the framework formed by the B^{dt}, B^{μ_2}, and B^{μ_3} atoms. The ratio within the hexagonal layer is one $B^{st,DTS}$ atom to one

(9) Schubert, K. *Kristallstrukturen zweikomponentiger Systeme*; Springer: Berlin, 1964; p 150 (in German).

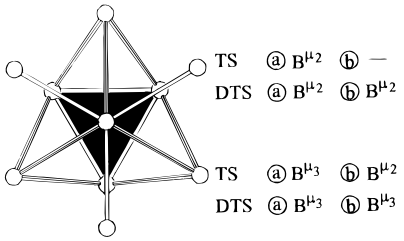

Figure 3. Projection of the cluster units shown in Figure 2 along the 3-fold axis. B^{μ_2} and B^{μ_3} atoms are situated at different heights above (a) or below (b) the center of a cluster unit. Their arrangement depends on the kind of cluster unit and, in case of a TS unit, additionally on the orientation of the central tetrahedron (fourth vertex above or below the center of the TS unit; the assignment in this figure refers to an orientation with the fourth vertex situated above the cluster center).

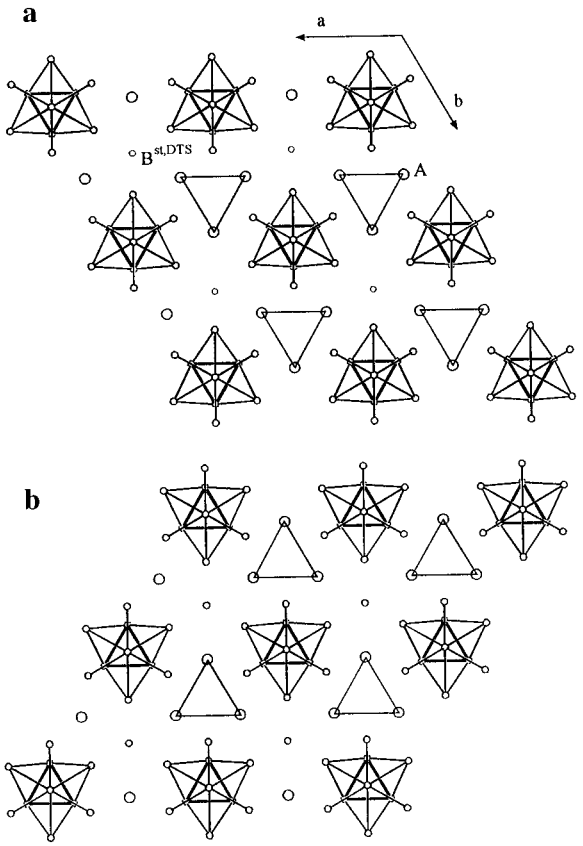

Figure 4. (a) Layer of hcp-arranged TS or DTS units (small circles) with triangles of A atoms (large circles). (b) Inverted arrangement of the layer shown in (a).

$B^{dt}_5B^{\mu_3}_6B^{\mu_2}_{6/2}$) cluster unit. The complete structures are built up by alternately stacking the hexagonal layer of Figure 4a with its inverted arrangement (Figure 4b) and connecting them via shared B^{μ_2} atoms. Consequently a layer of DTS introduces a block of *ABA* stacking with the two neighboring layers whereas a layer of TS leads to an *ABC* block (cf. Figure 3).

The base structure of the $EuMg_{5.2}$ structure type[4] consists of DTS layers with the composition A_3 ($B^{dt}_5B^{\mu_3}_6B^{\mu_2}_{6/2}$) $B^{st,DTS}$ (AB_5), and the deviation from the ideal stoichiometry is a consequence of a disordered arrangement of additional Mg atoms along the *c* axis on which all $B^{st,DTS}$ type atoms are situated.[3,4] Only A_3 cluster units (triangles) are possible with the *ABA* stacking sequence of DTS layers (Figure 5).

The building blocks of the Th_6Mn_{23} structure type[5] are TS layers, and the *ABC* stacking sequence allows the formation of A_6 octahedra within a double layer (Figure 6). Between two of such double layers, stuffing B atoms ($B^{st,TS}$) are situated

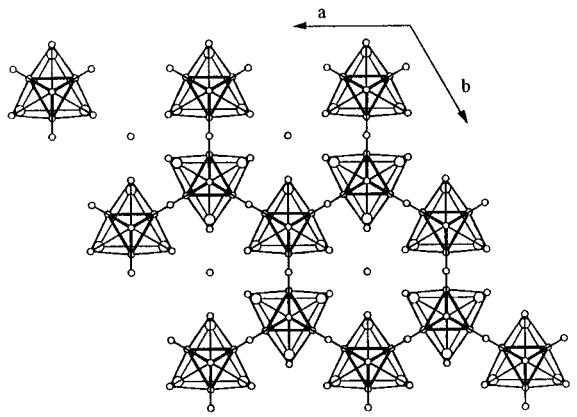

Figure 5. Stacking of two DTS layers in the structure of $EuMg_{5.2}$. (The obtained view is equivalent with the (100) projection of this structure.)

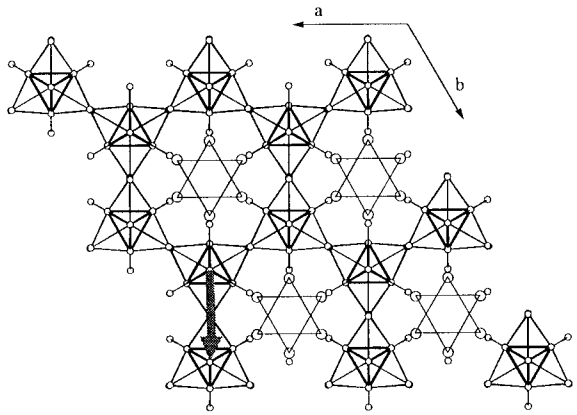

Figure 6. The stacking of two TS layers in Th_6Mn_{23} allows the formation of A_6 octahedra. The large gray arrow refers to a slip operation transforming the Th_6Mn_{23} structure into the $Ba_2Li_{4.21}Al_{4.79}$ structure (section 4.1.2.).

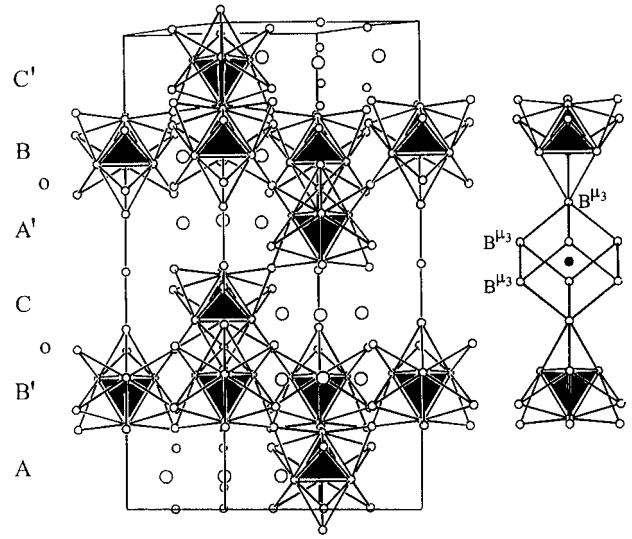

Figure 7. The cubic Th_6Mn_{23} structure in a rhombohedral setting with hexagonal axes of reference: TS layers and their inverted arrangement (indicated with primes) are stacked with an *AB′CA′BC′* sequence in *c* direction. Double layers containing A_6 octahedra (structure block shown in Figure 6) are marked with an o. The centers of the A_6 octahedra are situated on the planes (003). The right hand panel shows the coordination of a $B^{st,TS}$ atom (filled circle).

which are coordinated in a perfectly cubical manner by eight B^{μ_3} atoms from four consecutive TS layers (Figure 7). In the structure of Th_6Mn_{23} the ratio is one $B^{st,TS}$ atom to two $(B^t_4B^{\mu_3}_6B^{\mu_2}_{6/2})$ cluster units, and the composition of a TS double

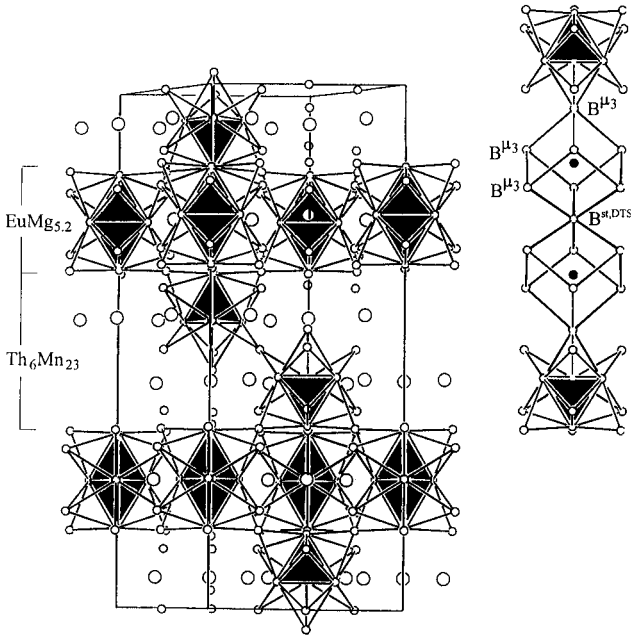

Figure 8. View of the unit cell of the Sr_3Mg_{13} structure formed by an alternate stacking of TS double layers (Th_6Mn_{23} structure blocks) and DTS layers ($EuMg_{5.2}$ structure blocks) in *c* direction. The right hand panel shows the coordination of two $B^{st,TS}$ atoms (filled circles).

layer containing A_6 clusters is $A_6(B^t_4B^{\mu_3}_4B^{\mu_2}_{6/2})_2B^{st,TS}_{2/2}$ (A_6B_{23}). The site of the layer linking B^{μ_2} atoms in this structure as well as in the $EuMg_{5.2}$ structure type is a center of inversion.

The Sr_3Mg_{13} structure type[3] is a perfect intergrowth of the Th_6Mn_{23} and $EuMg_{5.2}$ structure types with triangles and octahedra of A atoms. Double layers of TS and layers of DTS are alternately stacked, and the unit cell of Sr_3Mg_{13} (Figure 8), which contains two TS double layers $A_6(B^t_4B^{\mu_3}_4B^{\mu_2}_{6/2})_2B^{st,TS}_2$ and two DTS layers $A_3(B^{dt}_5B^{\mu_3}_6B^{\mu_2}_{6/2})B^{st,DTS}$, has the formula $A_{18}B_{78}$. Contrary to the Th_6Mn_{23} structure where the $B^{st,TS}$ atoms are shared between two double layers, the TS double layer in Sr_3Mg_{13} contains one $B^{st,TS}$ atom per TS unit. The coordination polyhedron of a $B^{st,TS}$ atom is a slightly distorted cube formed by seven B^{μ_3} atoms and one $B^{st,TS}$ atom (Figure 8, left hand panel).

3. Experimental Section

3.1. Synthesis. Samples of $Ca_6Li_{11}Al_{12}$, $Ba_2Li_{4.21}Al_{4.79}$, and $Sr_9Li_{17.5}Al_{25.5}$ were prepared by melting mixtures of the pure elements Li (99.9%, Aldrich), Al (99.9%, Aldrich), Ca (99.8%, Alfa), Sr (>99%, Alfa), and Ba (99.5%, Alfa) with a 5−10% excess of Al and Li in welded stainless stell ampoules under Ar atmosphere. According to differential thermoanalytical measurements the ternary compounds melt below 700 °C, and we performed syntheses by heating the samples to 800 °C within 2 h, keeping this temperature for 1 h, and finally cooling down slowly to room temperature (20−30 °C/h). All products were brittle and of gray color. Samples of $Ca_6Li_xAl_{23-x}$ were always accompanied by the binary compound $CaAl_2$, whereas X-ray powder patterns of the Sr/Li/Al and Ba/Li/Al samples with the composition corresponding to $Ba_2Li_{4.21}Al_{4.79}$ and $Sr_9Li_{17.5}Al_{25.5}$ did not exhibit byproducts to the ternary compounds. The latter compounds seem to exist with a fairly narrow phase width, which we conclude from the fact that in powder patterns of samples with different compositions and containing several phases, the positions of the lines belonging to $Ba_2Li_{3+x}Al_{6-x}$ and $Sr_9Li_{7+x}Al_{36-x}$ are only changed slightly. $Ca_6Li_xAl_{23-x}$ occurs with quite different values of *x*. When $11 < x < 13$ the cubic Th_6Mn_{23} structure is observed, but superstructure reflections may be found. For lower *x* values ($9 < x < 11$), a rhombohedral derivative structure of the basis type could be detected in addition to the cubic

Table 1. Crystal Data Summary for $Ca_6Li_{11}Al_{12}$, $Sr_9Li_{17.5}Al_{25.5}$, and $Ba_2Li_{4.21}Al_{4.79}$

formula	$Ca_6Li_{11}Al_{12}$	$Sr_9Li_{17.5}Al_{25.5}$	$Ba_2Li_{4.21}Al_{4.79}$
crystal size, mm^3	$0.25 \times 0.21 \times 0.13$	$0.17 \times 0.17 \times 0.08$	$0.08 \times 0.19 \times 0.29$
crystal system	cubic	hexagonal	rhombohedral
space group	$Fm\bar{3}m$	$P6_3/mmc$	$R\bar{3}m$
lattice constants, Å	$a = 13.430(2)$	$a = 9.638(4)$	$a = 9.946(10$
		$c = 27.586(6)$	$c = 26.992(3)$
volume, $Å^3$	2422.14	2219.18	2312.43
Z	4	2	9
calc density, g/cm^3	1.757	2.717	2.840
absorptions coeff, mm^{-1}	1.74	11.45	7.99
$F(000)$	1236	1668	1713
data collecn range, 2θ, deg	2−55	2−60	2−65
index range	$-17 \le h \le 17$	$0 \le h \le 13$	$-12 \le h \le 15$
	$-17 \le k \le 17$	$-6 \le k \le 11$	$-15 \le k \le 15$
	$0 \le l \le 17$	$0 \le l \le 38$	$0 \le l \le 40$
no. of reflcn measd	2912	3598	3706
no. of unique data	182 ($R_{int} = 0.054$)	1291 ($R_{int} = 0.053$)	1071 ($R_{int} = 0.048$)
no. of reflcn with $\|F\|^2 \ge 2\sigma(\|F\|^2)$	148	764	776
no. of reflcn for unit cell determ	92	26	66
2θ range, deg	21−35	33−52	21−40
absorption corr	empirical	no	empirical
extinction corr[a]	no	$\chi = 0.0016$ (2)	no
no. of params refined	22	76	54
goodness-of-fit on $\|F^2\|$	1.199	1.083	0.946
R values[b,c] $[\|F\|^2 \ge 2\sigma(\|F\|^2)]$	$R = 0.026$, $R_w = 0.052$	$R = 0.045$, $R_w = 0.085$	$R = 0.028$, $R_w = 0.042$
	$a = 0.0165$, $b = 5.09$	$a = 0.0349$, $b = 0$	$a = 0.0129$, $b = 0$
R values (all data)	$R = 0.038$, $R_w = 0.054$	$R = 0.105$, $R_w = 0.104$	$R = 0.051$, $R_w = 0.045$
largest hole and peak, $e/Å^3$	−0.25 and 0.50	−0.85 and 1.16	−1.33 and 0.89

[a] $F^* = F[1 + 0.002\chi F^2/\sin(2\theta)]^{1/4}$. [b] $R = [\sum(|F_o| - |F_c|)]/\sum|F_o|$. [c] $R_w = \{[\sum w(F_o^2 - F_c^2)^2]/\sum w(F_o^2)^2\}^{1/2}$. $w = [\sigma(|F_o|^2 + (aP)^2 + bP]^{-1}$. $P = (F_o^2(\ge 0) + 2F_c^2)/3$.

form.[10] The homogenity range of the three compounds has not been studied in detail yet.

3.2. Single-Crystal Structure Determination. All samples were highly crystalline, and suitable single crystals for structure determinations could easily be found. Intensity data sets for one crystal of each ternary compound were collected at room temperature with Mo Kα radiation (graphite monochromator) on a STOE, STADI 4 diffractometer (scan type $\omega-2\theta$). The details of the single-crystal data collection are listed in Table 1.

The crystal structures of $Ba_2Li_{3+x}Al_{6-x}$ and $Sr_9Li_{7+x}Al_{36-x}$ were solved using direct methods (program SHELXS-86[11]) and refined using full-matrix least-squares refinement on F^2 (program SHELXL-93[12]). Weak superstructure reflections were detected for the crystal of the compound $Ca_6Li_{11}Al_{12}$, indicating an 8-fold supercell of the cubic base structure. The Laue symmetry of the superstructure reflections is only $\bar{1}$. The superstructure could not be solved, but the cubic base structure was refined using the Th_6Mn_{23} structure as a model.

Refinement of site occupation factors revealed the occurrence of Al deficient sites in all three compounds. For these positions a mixed occupation of Li and Al atoms was assumed and the Li/Al ratio refined. The stoichiometry of the ternary compounds was determined from the refined Li/Al ratios.

3.3. Electronic Structure Calculation. All electronic structure calculations were performed within the framework of simple tight-binding (TB) Hückel or extended Hückel theory.[13] For the comparison of the structural stability of different network structures as a function of VEC, energy difference curves were calculated by the simple Hückel method (Figures 1 and 13). The network structures were considered as homonuclear, and orbital parameters of Al[14] were used for all B sites ($H_{3s3s} = 12.3$ eV, $H_{3p3p} = 6.5$ eV, $\zeta_{3s} = \zeta_{3p} = 1.167$). The electronic density of states of those structures whose structural stability was to be compared was scaled by an isotropic change of the bond lengths until their second moment adopted the same value.[15] (For second-moment scaling, see captions of Figures 1 and 13.) The simple cubic (sc) structure served as a neutral reference system,[16] and all energy difference curves were calculated relative to this structure. Atomic charges as a function of VEC were extracted from Mulliken population analyses using the extended Hückel method (Figure 14). The net charges can be used for the investigation of site preferences in network structures.[17]

Table 2. Positional and Equivalent Isotropic Displacement Parameters for $Ca_6Li_{11}Al_{12}$

atom	site	x	y	z	SOF	U_{iso}, 10^4 Å^2
Ca	24e	0.2033(1)	0	0	1	184(3)
M1 = $B^{st,TS}$	4b	0.5	0.5	0.5	Al 0.27(3)	303(44)
					Li 0.73(7)	
M2 = B^{μ_2}	24d	0	0.25	0.25	Al 0.63(1)	185(7)
					Li 0.37(1)	
M3 = B^{μ_3}	32f	0.3763(1)			Al 0.30(1)	193(12)
					Li 0.70(1)	
M4 = B^t	32f	0.1756(1)			Al 0.68(1)	153(6)
					Li 0.32(1)	

4. Results and Discussion

4.1. Description of the Crystal Structures. 4.1.1. $Ca_6Li_{11}Al_{12}$. The structure of $Ca_6Li_{11}Al_{12}$ is isotypic to the Th_6Mn_{23} type with mixed Li and Al occupancy for all four different sites of the B component. The atomic positions, site occupancies, and anisotropic displacement parameters are listed in Tables 2 and 3.

4.1.2. $Ba_2Li_{4.21}Al_{4.79}$. The structure of $Ba_2Li_{4.21}Al_{4.79}$ crystallizes with a novel structure type. Site occupancies and positional and anisotropic displacement parameters are given

(10) Nesper, R.; Curda, J. Unpublished results.
(11) Sheldrick, G. M. *SHELXS-86 Program for Solving Crystal Structures from Diffraction Data*; University of Göttingen: Göttingen, FRG, 1990.
(12) Sheldrick, G. M. *SHELXL-93 Program for the Refinement of Crystal Structures*; University of Göttingen: Göttingen, FRG, 1993.
(13) Wangbo, M. H.; Evain; M.; Hughbanks, T.; Kertesz, M.; Wijeyesekera, S.; Wilker, C.; Zheng, C.; Hoffmann, R. *Pogram EHMACC: Extended Hückel Molecular and Crystal Calculations; Program EHPC: Extended Hückel Property Calculations*, QCPE Version, 1987.
(14) Alvarez, S. *Tables of Atomic Parameters*; Dept. de Quimica Inorganica, Univ. Barcelona. Unpublished work.
(15) (a) Pettifor, D. G. *J. Phys. C: Solid State Phys.* **1986**, *19*, 285. (b) Pettifor, D. G.; Podloucky, R. *J. Phys. C: Solid State Phys.* **1986**, *19*, 315. (c) Lee, S; *Acc. Chem. Res.* **1991**, *24*, 249. (d) Lee, S.; Rousseau, R.; Wells, C. *Phys. Rev. B* **1992**, *46*, 12121.
(16) Häussermann, U.; Nesper, R. *J. Alloys Compd.* **1995**, *218*, 244.
(17) Nesper, R.; Miller, G. J. *J. Alloys Compd.* **1993**, *197*, 109.

Table 3. Anisotropic Displacement Parameters (10^4 Å^2) for $Ca_6Li_{11}Al_{12}$

atom	U_{11}	U_{22}	U_{33}	U_{12}	U_{13}	U_{23}
Ca	224(6)	164(4)	164(4)	0	0	0
M1	303(44)	303(44)	303(44)	0	0	0
M2	146(12)	205(9)	205(9)	0	0	10(10)
M3	193(12)	193(12)	193(12)	−12(8)	−12(8)	−12(8)
M4	153(6)	153(6)	153(6)	−4(4)	−4(4)	−4(4)

Table 4. Selected Bond Distances (n = Frequency) in $Ca_6Li_{11}Al_{12}$

atom pair	d (Å)	n	atom pair	d (Å)	n	atom pair	d (Å)	n
Ca−M3	3.305(2)	4	M2−M4	2.749(1)	4	M4−M2	2.749(1)	3
Ca−M4	3.356(1)	4	M2−M3	2.918(1)	4	M4−M4	2.825(2)	3
Ca−M2	3.416(1)	4	M2−Ca	3.416(1)	4	M4−M3	2.869(3)	3
Ca−Ca	3.861(2)	4				M4−Ca	3.356(1)	3
Ca−M1	3.985(1)		M3−M4	2.869(3)	3			
			M3−M1	2.878(2)				
M1−M3	2.878(2)	8	M3−M2	2.918(2)	3			
M1−Ca	3.985(1)	2	M3−Ca	3.305(3)	3			

Table 5. Positional and Equivalent Isotropic Displacement Parameters for $Ba_2Li_{4.21}Al_{4.79}$

atom	site	x	y	z	SOF	U_{iso}, 10^4 Å^2
Ba	18h	0.4753(1)	0.5247(1)	0.4274(1)	1	227(1)
Al1 = B^{μ_2}	18h	0.4905(1)	0.5095(1)	0.1842(1)	1	180(2)
Al2 = B^{μ_2}	9e	0.5	0	0	1	225(4)
M1 = B^{t}	6c	0	0	0.3363(1)	Al 0.63(1) Li 0.37(1)	198(9)
M2 = $B^{st,TS}$	3a	0	0	0	Al 0.80(2) Li 0.20(3)	323(15)
M3 = B^{t}	18h	0.4283(1)	0.5717(1)	0.0892(1)	Al 0.55(1) Li 0.45(1)	165(6)
Li1 = B^{μ_3}	3b	0	0	0.5	1	192(33)
Li2 = B^{μ_3}	18h	0.5017(4)	0.4983(4)	0.2999(3)	1	176(13)
Li3	6c	0	0	0.8773(7)	1	400(39)

Table 6. Anisotropic Displacement Parameters (10^4 Å^2) for $Ba_2Li_{4.21}Al_{4.79}$

atom	U_{11}	U_{22}	U_{33}	U_{12}	U_{13}	U_{23}
Ba	196(1)	196(1)	238(1)	60(1)	−28(1)	28(1)
Al1	176(4)	176(4)	188(6)	88(4)	−5(2)	5(2)
Al2	242(6)	213(8)	211(9)	107(4)	12(4)	24(7)
M1	197(11)	197(11)	198(18)	99(5)	0	0
M2	283(17)	283(17)	403(32)	141(8)	0	0
M3	172(7)	172(7)	165(10)	96(7)	3(3)	−3(3)
Li1	236(51)	236(51)	105(80)	118(25)	0	0
Li2	178(22)	178(22)	150(30)	73(25)	−19(13)	19(13)
Li3	304(49)	304(49)	594(119)	152(24)	0	0

in Tables 5 and 6. Figure 9 depicts a view of the unit cell of the rhombohedral structure in the hexagonal setting. When bonds are drawn between neighboring atoms both of fully occupied Al sites and mixed occupied Li/Al sites, hcp layers of icosahedra appear. The distorted icosahedra are formed by Al1 and M3 atoms and centered by the Li1 atoms. Within a layer (Figure 10) Li3 and Ba atoms are situated with triangles formed by the Ba atoms at heights below and above the centers of the icosahedra. The layers are stacked in an *ABC* sequence and connected via M1 and Al2 atoms. Additional Li (Li2) and M atoms (M2) are located between the layers. The icosahedral unit in the structure of $Ba_2Li_{4.21}Al_{4.79}$ can be divided in two ($B^{t}_4B^{\mu_3}_6B^{\mu_2}_6$) clusters (shown in Figure 2) sharing one B^{μ_3} atom (Figure 11). The central tetrahedron of the TS is built by M1 and M3 atoms, and the faces are capped by the Li1 (shared) and the Li2 atoms. All edges are bridged by Al atoms. The Al1 atoms together with the M3 atoms build the distorted icosahedron, and the Al2 atoms link neighboring layers analogous to the B^{μ_2} atoms in the Th_6Mn_{23} structure. The whole structure of $Ba_2Li_{4.21}Al_{4.79}$ can simply be derived from the Th_6Mn_{23} structure type by a slip[18] of TS layers within the double layers containing A_6 octahedra (shown in Figure 6, cf. Figure 7). The operation is a translation by the vector ($^1/_3$,$^2/_3$,0) in every plane (003)[19] in the Th_6Mn_{23} structure, referring to the rhombohedral setting with hexagonal axes of reference (Figure 7). Within the double layers, TS units can then be connected by shared B^{μ_3} atoms and thus form icosahedra. The linkage between two double layers remains unchanged. The $B^{st,TS}$ position in the Th_6Mn_{23} structure corresponds to the M2 position in the $Ba_2Li_{4.21}Al_{4.79}$ structure. The slip operation changes the coordination polyhedron of this atom from a cube to a compressed octahedron by removing two opposite vertices of

Table 7. Selected Bond Distances (n = Frequency) in $Ba_2Li_{4.21}Al_{4.79}$

atom pair	d (Å)	n	atom pair	d (Å)	n	atom pair	d (Å)	n
Ba−Li3	3.386(5)		A12−M3	2.707(2)	2	Li1−M3	2.654(2)	6
Ba−Li2	3.470(8)		Al2−M1	2.872(1)	2	Li1−Al1	2.748(1)	6
Ba−Li2	3.501(5)	2	Al2−Li2	3.023(4)	4			
Ba−Al1	3.505(1)	2				Li2−M3	2.934(6)	2
Ba−M3	3.580(1)	2	M1−M3	2.845(2)	3	Li2−M2	2.983(5)	
Ba−M1	3.584(1)		M1−Al2	2.872(1)	3	Li2−M1	3.013(5)	
Ba−Al2	3.694(1)	2	M1−Li2	3.013(5)	3	Li2−Al2	3.023(4)	2
Ba−Al1	3.700(1)	2				Li2−Al1	3.130(8)	
Ba−Li3	3.986(16)		M2−Li2	2.983(5)	6	Li2−Li2	3.367(10)	2
Ba−Ba	4.011(1)		M2−Li3	3.311(20)	2	Li2−Ba	3.470(8)	
Ba−M2	4.161(1)					Li2−Ba	3.501(5)	2
Ba−Ba	4.236(1)	2	M3−Li1	2.654(2)				
			M3−Al2	2.707(2)		Li3−Al1	3.119(5)	3
Al1−Li1	2.748(1)		M3−Al1	2.778(2)		Li3−M2	3.311(20)	
Al1−M3	2.778(2)		M3−M3	2.833(2)	2	Li3−Ba	3.386(5)	3
Al1−M3	2.862(2)	2	M3−M1	2.845(2)				
Al1−Al1	2.867(1)	2	M3−Al1	2.862(2)	2			
Al1−Li3	3.119(5)		M3−Li2	2.934(6)	2			
Al1−Li2	3.130(8)							

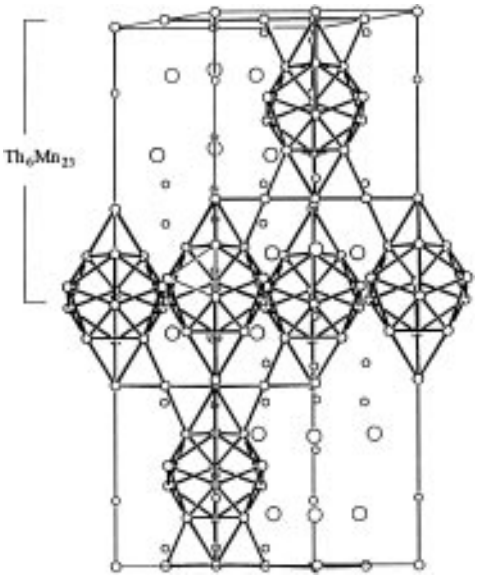

Figure 9. View of the unit cell with hexagonal axes of reference for $Ba_2Li_{4.21}Al_{4.79}$. Large circles represent Ba, medium-sized circles Al and M, and small circles Li atoms. Bonds are drawn between neighboring Al and M atoms. M and Al atoms form hcp layers of icosahedra which are stacked in *c* direction with *ABC* sequence. Alternatively the structure consists of Th_6Mn_{23} structure blocks (TS double layers only containing A_3 triangles, cf. Figure 7).

(18) Hyde, B. G.; Andersson, S. *Inorganic Crystal Structures*; John Wiley & Sons: New York, 1989.

(19) It could also be the vector ($^2/_3$,$^1/_3$,0), dependent on which part of the structure is moved by the slip operation.

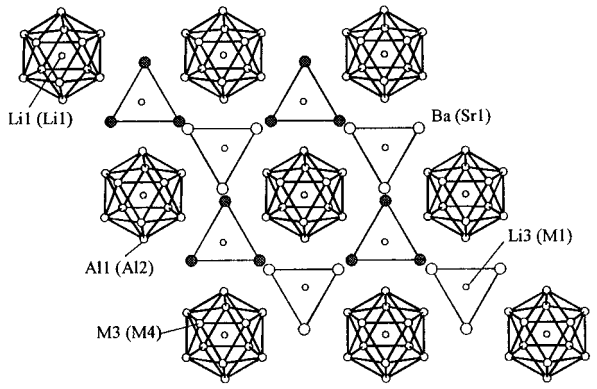

Figure 10. Layer of hcp-arranged (M,Al) icosahedra in $Ba_2Li_{4.21}Al_{4.79}$ and $Sr_9Li_{17.5}Al_{25.5}$. The icosahedra are centered by Li atoms. Large circles represent the alkaline earth metal atoms A. The circles are shaded for A atoms situated above and open for A atoms situated below the center of the icosahedra. Atomic positions in parentheses refer to the $Sr_9Li_{17.5}Al_{25.5}$ structure. Note that this layer is obtained by a slip process from the TS double layer shown in Figure 6.

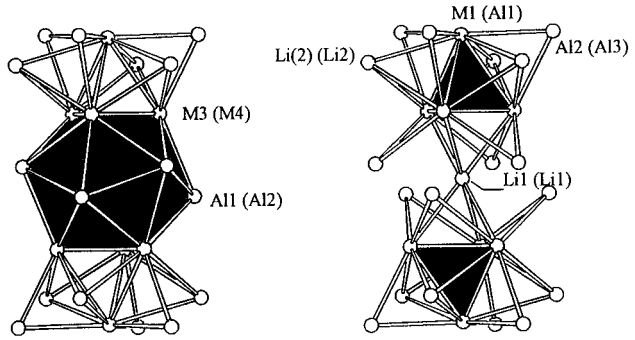

Figure 11. Duality of the icosahedral unit in the structures of $Ba_2Li_{4.21}Al_{4.79}$ and $Sr_9Li_{17.5}Al_{25.5}$ and two $B_4^tB_4^{\mu_3}B_6^{\mu_2}$ clusters (shown in Figure 1) sharing one B^{μ_3} atom. The labels in parentheses refer to atomic positions in the $Sr_9Li_{17.5}Al_{25.5}$ structure.

the cube (compare right part of Figure 8). The octahedron is formed by six Li2 atoms. The only position introduced additionally in the structure of $Ba_2Li_{4.21}Al_{4.79}$ are the Li3 atoms situated between three icosahedra (Figure 10).

4.1.3. $Sr_9Li_{17.5}Al_{25.5}$. In the hexagonal structure of $Sr_9Li_{17.5}Al_{25.5}$, hcp layers of icosahedra and DTS are alternately stacked in the *c* direction with the sequence $A\beta A\gamma$ (Greek letters refer to DTS layers; see Figure 12). Site occupancies and positional and anisotropic displacement parameters are summarized in Tables 8 and 9. The structure of $Sr_9Li_{17.5}Al_{25.5}$ can be derived from the Sr_3Mg_{13} structure type (Figure 8) in the same way as the structure of $Ba_2Li_{4.21}Al_{4.79}$ can be derived from the Th_6Mn_{23} structure type. The icosahedra-forming slip operation is a translation by the vector $(^1/_3,^2/_3,0)$ in every plane (002)[19] in the Sr_3Mg_{13} structure. Alternatively, the $Sr_9Li_{17.5}Al_{25.5}$ structure can be regarded as a perfect intergrowth between the $Ba_2Li_{4.21}Al_{4.79}$ and the $EuMg_{5.2}$ structure types. The icosahedra are formed by the Al2 and M4 atoms (corresponding to the Al1 and M3 atoms in $Ba_2Li_{4.21}Al_{4.79}$) and centered by the Li1 atoms (Figures 10 and 11). The distance between two Sr1 atoms in a Sr_3 triangle is 4.07 Å, whereas the corresponding Ba−Ba distance in $Ba_2Li_{4.21}Al_{4.79}$ is 4.24 Å. This difference directly affects the distances between the centers of the icosahedra and thus the lattice constant of the *a* axes.

The DTS clusters consist of the atoms M6 ($B^{dt,eq}$, equatorial position in the trigonal bipyramid), M7 ($B^{dt,ax}$, axial position in the trigonal bipyramid), and M5 (B^{μ_3}). Edges between the equatorial and axial positions are bridged by Al3 atoms which link the hcp layers of DTS and icosahedra. The M2 atoms have the position of the $B^{st,DTS}$ atoms in the DTS layers. The M3 site in the structure of $Sr_9Li_{17.5}Al_{25.5}$ is coordinated by seven atoms (three Li2, three M5, one M2) and corresponds to the $B^{st,TS}$ position in the Sr_3Mg_{13} structure type. The coordination polyhedron can be derived from a distorted cube by removing one vertex (through the slip operation, cf. Figure 8). Only the position M1 has no correspondence to the Sr_3Mg_{13} structure.

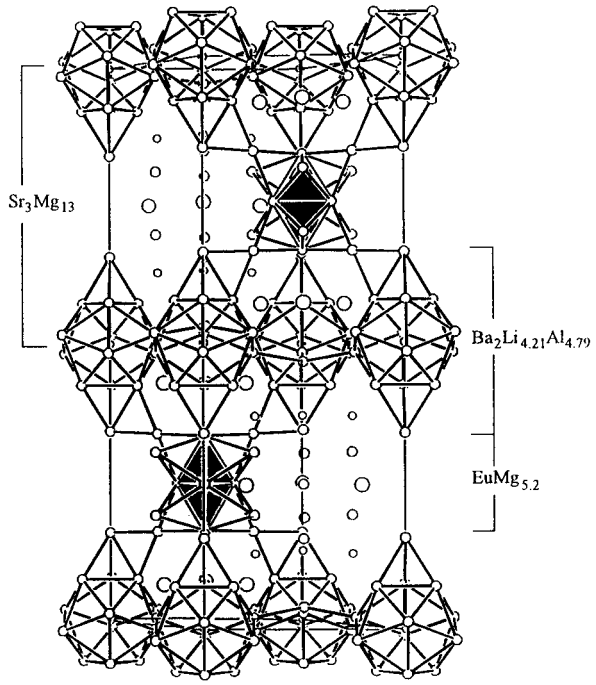

Figure 12. View of the unit cell for $Sr_9Li_{17.5}Al_{25.5}$ showing hcp layers of icosahedra and DTS formed by Al and M atoms. The two different kinds of layers are stacked alternately. Large circles represent Sr, medium-sized circles Al and M, and small circles Li atoms.

Table 8. Positional and Equivalent Isotropic Displacement Parameters for $Sr_9Li_{17.5}Al_{25.5}$

atom	site	*x*	*y*	*z*	SOF	U_{iso}, 10^4 Å^2
Sr1	12k	0.5258(1)	0.0517(1)	0.0707(1)	1	130(2)
Sr2	6h	0.1401(1)	0.2802(2)	$^1/_4$	1	116(3)
Al1 = B^t	4e	0	0	0.1589(2)	1	209(12)
Al2 = B^{μ_2}	12k	0.1623(4)	0.3247(2)	0.0169(1)	1	218(8)
Al3 = B^{μ_2}	12k	0.1682(2)	0.3365(3)	0.6621(1)	1	118(6)
M1	4f	$^1/_3$	$^2/_3$	0.0328(3)	Al 0.48(2) Li 0.52(3)	186(30)
M2 = $B^{st,DTS}$	2c	$^1/_3$	$^2/_3$	$^1/_4$	Al 0.30(4) Li 0.70(4)	388(80)
M3 = $B^{st,TS}$	4f	$^1/_3$	$^2/_3$	0.1544(3)	Al 0.49(3) Li 0.51(3)	210(32)
M4 = B^t	12k	0.0969(3)	0.1938(5)	0.5750(1)	Al 0.56(1) Li 0.44(1)	85(12)
M5 = B^{μ_3}	12k	0.5012(3)	0.0024(6)	0.6940(1)	Al 0.63(1) Li 0.37(1)	165(13)
M6 = $B^{dt,eq}$	6h	0.7633(4)	0.5267(8)	$^1/_4$	Al 0.55(2) Li 0.45(2)	121(18)
M7 = $B^{dt,ax}$	4f	$^1/_3$	$^2/_3$	0.6657(6)	Al 0.23(3) Li 0.77(3)	378(71)
Li1 = B^{μ_3}	2a	0	0	0	1	126(78)
Li2 = B^{μ_3}	12k	0.1696(9)	0.339(2)	0.1290(5)	1	155(36)

4.2. Tight-Binding Energy Differences of the B Substructures. Figure 13a shows the energy difference curves of the B substructures in the structure types of Th_6Mn_{23} ($Ca_6(Li,Al)_{23}$), Sr_3Mg_{13}, $Sr_9(Li,Al)_{43}$, and $Ba_2(Li,Al)_9$. All curves have a pronounced maximum which indicates the important role of the VEC in controlling structural stability of these different networks. The maxima lie in the narrow range between 2.45 and 2.6 electrons per network atom. When applying a formal

Table 9. Anisotropic Displacement Parameters (10^4 Å^2) for $Sr_9Li_{17.5}Al_{25.5}$

atom	U_{11}	U_{22}	U_{33}	U_{12}	U_{13}	U_{23}
Sr1	108(3)	169(5)	135(3)	84(2)	15(2)	30(4)
Sr2	100(4)	126(7)	132(5)	63(3)	0	0
Al1	181(17)	181(17)	265(28)	90(8)	0	0
Al2	180(18)	213(15)	249(15)	90(9)	8(12)	4(6)
Al3	129(10)	104(13)	114(11)	52(6)	−16(5)	−33(9)
M1	97(34)	97(34)	362(60)	49(17)	0	0
M2	353(97)	353(97)	457(144)	176(49)	0	0
M3	150(34)	150(34)	329(62)	75(17)	0	0
M4	84(16)	76(20)	93(19)	38(10)	2(8)	3(15)
M5	157(18)	168(23)	175(20)	84(12)	−11(8)	−22(16)
M6	135(28)	105(34)	113(29)	53(17)	0	0
M7	341(80)	341(80)	454(129)	171(40)	0	0
Li1	150(124)	150(124)	80(167)	75(62)	0	0
Li2	133(61)	140(81)	193(69)	70(40)	−22(30)	−43(59)

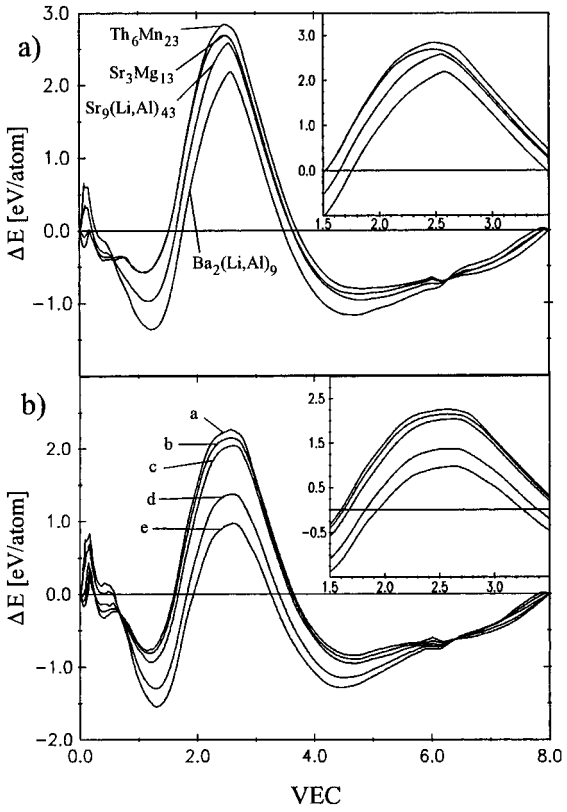

Figure 13. (a) TB energy difference curves vs VEC for the B substructures in Th_6Mn_{23}, Sr_3Mg_{13}, $Sr_9(Li,Al)_{43}$, $Ba_2(Li,Al)_9$, and the simple cubic structure as a reference. For positive values of ΔE, a B substructure is more stable than the reference structure. (b) Energy difference curves for B substructures without stuffing B^{st} atoms in Th_6Mn_{23} (curve a), Sr_3Mg_{13} (curve b), $EuMg_{5.2}$ (curve c), $Sr_9(Li,Al)_{43}$ (curve d), and $Ba_2(Li,Al)_9$ (curve e). The chosen reference value of the second moment[15] was that for the B substructure in $Ca_6Li_{11}Al_{12}$ (Th_6Mn_{23} structure type).

electron transfer from the A component to the B atoms, one obtains from the composition of the four compounds the following VECs for their B substructures: $Ca_6Li_{11}Al_{12}$, 2.57, Sr_3Mg_{13} 2.46, $Sr_9Li_{17.5}Al_{25.5}$ 2.60, and $Ba_2Li_{4.21}Al_{4.79}$, 2.51. These values are very close to the maxima of the corresponding energy difference curves. The absolute amplitudes of these curves cannot be used for comparing the structural stability of the total structures because the A atoms were neglected in this kind of analysis.[16] The stuffing B^{st} atoms have only a slight influence on the location of the maxima of the energy difference curves. Figure 13b shows the curves of the networks derived from the B substructures in Th_6Mn_{23} (curve a), Sr_3Mg_{13} (curve b), $EuMg_{5.2}$ (curve c), $Sr_9(Li,Al)_{43}$ (curve d), and $Ba_2(Li,Al)_9$ (curve e) by removing all B^{st} atoms. Remarkably, the shape of the curves is almost independent of the kind of basis cluster (TS or DTS) the network is built of (curves a−c) and of the kind of linkage (via B^{μ_2} or B^{μ_3} atoms) of these basis clusters in the network (curves d, e). From an electronical point of view the different B substructures appear as equivalent solutions. Similar to Zintl phases, this class of intermetallic compounds shows a diversity of substructures for a certain optimum value of VEC, and factors like the size of the A atoms and packing effects determine the final structure.

4.3. Distances and Site Occupancies in the B Substructures. The positions of the B substructures in the Th_6Mn_{23} structure are contrarily polarized and can be differentiated in ternary compounds. In $Ca_6Li_{11}Al_{12}$ the B^{μ_2} (M2) and B^t (M4) positions are preferably occupied by Al atoms (63% and 68%, respectively) and the B^{μ_3} (M3) and $B^{st,TS}$ (M1) by Li atoms (70% and 73%, respectively). The nearest neighbor distances in the B substructure are 2.83 Å (B^t-B^t), 2.75 Å ($B^t-B^{\mu_2}$), 2.87 Å ($B^t-B^{\mu_3}$), and 2.88 Å ($B^{st,TS}-B^{\mu_3}$) (Table 4). For comparison, the Al−Al, Li−Al, and Li−Li distances in the Zintl phase LiAl,[20] where Li atoms as well as Al atoms form a diamond substructure, are 2.76 Å. Figure 14a shows the calculated net charges on the different positions of the B substructure in Th_6Mn_{23} ($Ca_6Li_{11}Al_{12}$) as a function of VEC. The charges on the B^{μ_2} and B^{μ_3} position are correlated contrarily in a way that the B^{μ_2} position is negatively polarized and the B^{μ_3} position positively polarized. This corresponds to the site occupancies found for the B^{μ_2} and B^{μ_3} position or to the distribution of Li and Al atoms. According to the population analysis, the $B^{st,TS}$ position is negatively polarized. This seems to be sensible, because the $B^{st,TS}$ atoms are coordinated by eight (positively polarized) B^{μ_3} atoms. However, in the compound $Ca_6Li_{11}Al_{12}$, this position is preferably occupied by the more electropositive Li atoms.

The formation of icosahedral units in the structures of $Ba_2Li_{4.21}Al_{4.79}$ and $Sr_9Li_{17.5}Al_{25.5}$ causes considerable deviations in the bond distances compared to those of the idealized structures of Th_6Mn_{23} and Sr_3Mg_{13}, respectively (Tables 7 and 10). The distances between the B^t atoms and the TS connecting (icosahedra centering) B^{μ_3} atoms are very short (2.65 Å in $Ba_2Li_{4.21}Al_{4.79}$ and 2.63 Å in $Sr_9Li_{17.5}Al_{25.5}$) compared to the other set of $B^t-B^{\mu_3}$ distances (between 2.93 and 3.01 Å in $Ba_2Li_{4.21}Al_{4.79}$ and between 2.88 and 2.95 Å in $Sr_9Li_{17.5}Al_{25.5}$). The $B^t-B^{\mu_2}$ distances vary between 2.71 and 2.86 Å in $Ba_2Li_{4.21}Al_{4.79}$ and between 2.68 and 2.86 Å in $Sr_9Li_{17.5}Al_{25.5}$. The B^t-B^t distances are fairly constant, ranging from 2.83 to 2.85 Å in $Ba_2Li_{4.21}Al_{4.79}$ and from 2.80 to 2.82 Å in $Sr_9Li_{17.5}Al_{25.5}$. The differentiation of the B^{μ_2} and B^{μ_3} position is complete in the icosahedral units of these two compounds because the B^{μ_2} positions are fully occupied by Al atoms and the B^{μ_3} positions by Li atoms. The B^t position that is part of the icosahedron is in both structures and almost equally occupied by Li and Al (M3 in $Ba_2Li_{4.21}Al_{4.79}$ and M4 in $Sr_9Li_{17.5}Al_{25.5}$). The other B^t position is preferably occupied by Al atoms in $Ba_2Li_{4.21}Al_{4.79}$ (M1, 63%) and is a fully occupied Al position in $Sr_9Li_{17.5}Al_{25.5}$ (Al1). Figure 14b shows the calculated net charges on the positions involved in TS forming and linking in the structure of $Ba_2Li_{4.21}Al_{4.79}$. Again, the net charges for the B^{μ_2} and B^{μ_3} atoms correspond with the observed site occupancies around a VEC of 2.5−2.6, whereas those for the B^t sites appear positively polarized in contradiction to the experimental result.

In the DTS layer of the $Sr_9Li_{17.5}Al_{25.5}$ structure, the $B^{dt}-B^{dt}$ distances vary between 2.80 and 2.83 Å, while the $B^{dt}-B^{\mu_2}$

(20) Levine, E. D.; Rapperport, E. J. *Trans. Metall. Soc. AIME* **1963**, *227*, 1204.

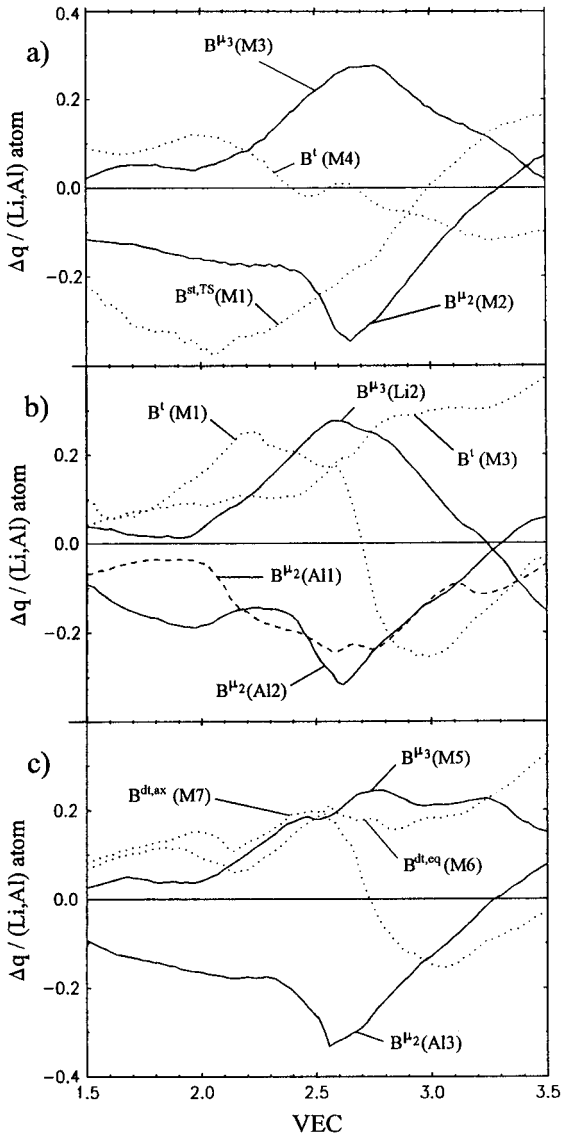

Figure 14. Net charges from Mulliken populations as a function of VEC for (a) B atoms in the compound $Ca_6Li_{11}Al_{12}$ (Th_6Mn_{23} structure type) and (b) B atoms forming the icosahedral units in the structure of $Ba_2Li_{4.21}Al_{4.79}$. (The icosahedron centering position B^{μ_3} (Li1) is highly positively polarized and its curve is excluded. The Δq curves for the corresponding positions in $Sr_9Li_{17.5}Al_{25.5}$ are almost identical.) Net charges from Mulliken populations as a function of VEC for (c) B atoms forming DTS units in the structure of $Sr_9Li_{17.5}Al_{25.5}$. Some curves are dotted for clarity.

distances are shorter, ranging from 2.68 to 2.76 Å, and the B^{dt}—B^{μ_3} contacts are longer, ranging from 2.89 to 2.91 Å. The axial position of the trigonal bipyramid (M7) is mainly occupied by Li atoms (77%), and the equatorial position (M6) is occupied almost equally by Li and Al atoms. In contrast to the TS units, the face-capping B^{μ_3} position of the M5 atoms is preferably occupied by the more electronegative Al atoms. The calculated net charges for the positions of a DTS layer in the structure of $Sr_9Li_{17.5}Al_{25.5}$ (Figure 14c) do not corroborate these findings. The three positions of a DTS appear at a VEC around 2.5 not differently polarized.

Apparently the calculated net charges as a function of VEC are only a very qualitative tool for investigating site occupancies. One can think of several reasons for the observed discrepancies: Besides the assumption that the more electronegative atoms segregate on a negatively polarized site, there are severe approximations in the theoretical model, like the neglection of the A component, its semiempirical nature, and the definition of the net charges. On the experimental site annealing temperature and time might influence the occupation of a position. However, a general trend could be established, namely the positive polarization of B^{μ_3} and the negative polarization of B^{μ_2} sites, which is also reflected by the observed site occupancies.

Table 10. Selected Bond Distances (n = Frequency) in $Sr_9Li_{17.5}Al_{25.5}$

atom pair	*d* (Å)	*n*	atom pair	*d* (Å)	*n*	atom pair	*d* (Å)	*n*
Sr1−M1	3.379(3)		Al3−M6	2.680(4)		M4−Li1	2.627(4)	
Sr1−Al2	3.392(3)	2	Al3−M4	2.681(5)		M4−Al3	2.681(5)	
Sr1−Li2	3.406(16)	2	Al3−M7	2.758(3)		M4−Al2	2.761(5)	
Sr1−M5	3.431(4)		Al3−Al1	2.810(3)		M4−M4	2.802(7)	2
Sr1−M4	3.441(5)	2	Al3−M5	2.915(6)	2	M4−Al1	2.823(6)	
Sr1−M7	3.520(13)		Al3−Li2	2.964(18)	2	Mr−Al2	2.855(5)	2
Sr1−Al2	3.578(3)	2				M4−Li2	2.877(18)	2
Sr1−Al3	3.606(3)	2	Li1−M4	2.627(4)	6	M4−Sr1	3.441(5)	2
Sr1−M1	3.699(8)		Li1−Al2	2.750(3)	6			
Sr1−M3	3.957(6)					M5−M6	2.885(6)	2
Sr1−Sr1	3.994(2)		Li2−M3	2.821(16)		M5−M7	2.909(7)	
Sr1−Sr1	4.072(2)	2	Li2−M4	2.877(18)	2	M5−Al3	2.915(6)	2
			Li2−Al1	2.949(16)		M5−M3	2.970(6)	
Sr2−M2	3.225(2)		Li2−Al3	2.964(18)	2	M5−M5	3.091(8)	
Sr2−Li2	3.373(14)	2	Li2−Al2	3.096(15)		M5−M2	3.165(5)	
Sr2−M5	3.393(5)	4	Li2−M5	3.280(17)	2	M5−Li2	3.280(17)	2
Sr2−Al1	3.434(4)	2	Li2−Sr2	3.373(14)		M5−Sr2	3.393(5)	2
Sr2−M6	3.441(8)	2	Li2−Sr1	3.406(16)	2	M5−Sr1	3.431(4)	
Sr2−Al3	3.559(3)	4						
Sr2−Sr2	4.052(3)	2	M1−Al2	2.888(4)	3	M6−Al3	2.680(4)	2
Sr2−M3	4.166(6)	2	M1−M3	3.353(14)		M6−M6	2.795(11)	2
			M1−Sr1	3.379(3)	3	M6−M7	2.832(15)	2
Al1−Al3	2.810(3)	3				M6−M5	2.885(7)	4
Al1−M4	2.823(6)	3	M2−M3	2.637(9)	2	M6−Sr2	3.441(8)	2
Al1−Li2	2.949(16)	3	M2−M5	3.165(5)	6			
Al1−Sr2	3.434(4)	3	M2−Sr2	3.225(2)	3	M7−Al3	2.758(3)	3
						M7−M6	2.832(15)	3
Al2−Li1	2.750(3)		M3−M2	2.637(9)		M7−M5	2.909(7)	3
Al2−M4	2.761(5)		M3−Li2	2.821(16)	3			
Al2−M4	2.855(5)	2	M3−M5	2.970(6)	3			
Al2−Al2	2.866(7)	2	M3−M1	3.353(14)				
Al2−M1	2.888(4)							
Al2−Li2	3.096(15)							
Al2−Sr1	3.392(3)	2						

5. Conclusion

The novel structures of $Sr_9Li_{7+x}Al_{36-x}$ and $Ba_2Li_{3+x}Al_{6-x}$ are further examples of a family of intermetallic compounds A_mB_n where the partial structure of the B component is built up by the basis clusters TS and DTS and the heavier A atoms form polynuclear units. The unique building block of the complete structure is an hcp layer of TS or DTS with triangles of A atoms. The structures are formed by stacking these hexagonal layers in *c* direction. The origin of the structural diversity lies in the possibility of connecting these layers differently. In the structure types Th_6Mn_{23}, $EuMg_{5.2}$, and Sr_3Mg_{13}, the two-dimensional building blocks are exclusively linked by atoms bridging edges of the basis clusters, whereas in the structures of the ternary compounds $Ba_2Li_{4.21}Al_{4.79}$ and $Sr_9Li_{17.5}Al_{25.5}$, TS clusters may also be connected by sharing face-capping B^{μ_3} atoms, thus forming isolated icosahedral units. The possibility of differentiating between atomic positions in the B substructures by the variable (Li/Al) site occupancies enlarges the structural flexibility of the ternary compounds.

The VEC has a strong influence on the structural stability for the sp-bonded B substructures in these structure types. The stability maxima are found at about 2.5 electrons per B atom. For the compounds $Ca_6Li_{11}Al_{12}$, $Ba_2Li_{4.21}Al_{4.79}$, and $Sr_9Li_{17.5}Al_{25.5}$, the VECs for the B (Li,Al) substructures come very close to this value when assuming an electron transfer from the A component. The application of this formal charge transfer and the possible division of the total structures in an A cluster part

and a B substructure is similar to Zintl phases, which formally consist of A cations and a polyanionic B framework. In Zintl phases the B substructure fulfils the octet rule, and the relationship between geometrical structure and VEC is expressed in the Zintl−Klemm concept. Binary Zintl phases are formed between an alkali or alkaline earth metal being the A component and a more electronegative metametal, e.g. Si or Ge. By reducing the electronegativity difference between the main group A and B components step by step, one can describe a structural route from valence compounds with open B frameworks (Zintl phases) to close-packed intermetallic compounds like $CaLi_2$, $CaMg_2$, KNa_2, or CsK_2[6] crystallizing in the structure of the hexagonal Laves phase ($MgZn_2$ structure type). The link on the side of the valence compounds is the family of polar intermetallic compounds formed between alkali or alkaline earth metals and a metallic group 13 element (i.e. Al, Ga, or In). Although polyanionic substructures with short distances between the B atoms are still present, these compounds usually do not obey the octet rule. As a result of our investigations we want to interpret the family of the discussed structure types with a rather dense B network surrounding A cluster units as the link on the side of the close-packed compounds (cf. Figure 1).

Acknowledgment. This research was supported by the Swiss National Science Foundation (Schweizerischer Nationalfonds). U.H. acknowledges a Feodor-Lynen Fellowship of the A. v. Humboldt Foundation.

JA961127K